

# Signal-to-noise ratio in dual-gated Si nanowire FET sensors

A. Tarasov,\* W. Fu,\* O. Knopfmacher, J. Brunner, M. Calame, and C. Schönenberger†  
*Department of Physics, University of Basel, Klingelbergstrasse 82, CH-4056 Basel, Switzerland*  
 (Dated: September 16, 2022)

Recent studies on nanoscale FET sensors reveal the crucial importance of the low frequency noise for determining the ultimate detection limit. In this letter, the  $1/f$ -type noise of Si nanowire (NW) FET sensors is investigated. We demonstrate by using a dual-gated approach that the signal-to-noise ratio (SNR) can be increased by almost two orders of magnitude if the NW-FET is operated in an optimal gate voltage range. In this case, the additional noise contribution from the contact regions is minimized, and an accuracy of 0.5 ‰ of a pH shift in one Hz bandwidth can be reached.

PACS numbers: 73.61.Cw, 73.40.Mr

During the past decade, there has been a growing interest in applying the concept of an ion-sensitive field effect transistor (ISFET)<sup>1,2</sup> to nanoscale devices. It has been shown that carbon nanotube (CNT)<sup>3–6</sup>, graphene<sup>7–9</sup>, and nanowire (NW) FETs<sup>10–12</sup> are especially promising for sensing applications. Compared to conventional FETs, nanoscaled devices provide a larger surface-to-volume ratio. This results in a high sensitivity of the overall FET channel conductance to changes in the surface potential caused by the adsorption of molecules<sup>13</sup>. In order to reach the detection limit, intense attempts have recently been made to understand the factors determining the signal-to-noise ratio (SNR)<sup>9,14–16</sup>. Studies on CNT FETs<sup>15</sup> and on NW<sup>16</sup> showed that the SNR increases in the subthreshold regime, which is therefore the preferred regime for high sensitivity. However, a more detailed understanding of the noise properties is needed to optimize the SNR across the full operating range of the FET.

In the present work, we measure the low-frequency  $1/f$  noise of a dual-gated<sup>15,17–19</sup> NW-FET in ambient and in a buffer solution and determine the resolution limit expressed in a noise equivalent threshold voltage shift  $\delta V_{th}$ , the latter being the measurement quantity in these types of sensors. We identify two regimes which differ in the relative importance of the contact and intrinsic NW resistance. The lowest value in  $\delta V_{th}$  is found when the working point of the NW-FET is adjusted such that the intrinsic NW resistance dominates. In the other case when the contact resistance dominates the noise can be larger by almost two orders of magnitude for nominally the same overall resistance. This result shows the importance of being able to adjust the operating point properly. In the best possible case we determine a resolution limit of 0.5 ‰ of a pH change in one Hz bandwidth, which is comparable to a commercial pH meter (0.1 ‰<sup>20</sup>), but for a much smaller active sensing area.

Silicon NW-FETs were produced by UV lithography according to the top-down approach which was previously described in detail<sup>19</sup>. This high-yield process provides reproducible, hysteresis-free NW-FETs with the following dimensions: length  $\times$  width  $\times$  height = 10  $\mu\text{m}$   $\times$  700 nm  $\times$  80 nm (Fig. 1a). A thin  $\text{Al}_2\text{O}_3$  layer was deposited on the device to ensure leakage-free operation in an electrolyte solution. In addition, a liquid channel was

formed in a photoresist layer, reducing the total area exposed to the electrolyte.

The measurement setup is schematically shown in Fig. 1b. The NWs were operated at low source-drain DC voltages  $V_{sd} = 10 - 100 \text{ mV}$  in the linear regime. The source-drain current  $I_{sd}$  through the NW was measured by a current-voltage converter with a variable gain ( $10^5 - 10^9 \text{ V/A}$ ). The conductance  $G$  of the NW-FET is then obtained as the ratio  $G = I_{sd}/V_{sd}$  while varying both the back-gate  $V_{bg}$  and liquid gate voltage  $V_{lg}$ . This yields a two-dimensional (2D) conductance map, as shown in Fig. 1c<sup>19</sup>. The vertical axis  $V_{ref}$  is the potential of the liquid, as measured by a calomel reference electrode. The equivalent voltage noise power spectral density  $S_V$  (see e.g.<sup>22</sup>) was determined along the solid white lines through a fast Fourier transform of the time dependent fluctuations of  $I_{sd}$ .

The conductance map in Fig. 1c displays two different regimes, above and below the white dashed line at about  $V_{ref} = +0.4 \text{ V}$ , which differ in their relative coupling to the two gates. This is visible in the slopes  $s = \partial V_{ref}/\partial V_{bg}$  (short white lines and numbers), determined at constant  $G$ , that represent the ratio of the gate coupling capacitances  $C_{bg}/C_{lg}$ , where  $C_{bg}$  denotes the back-gate and  $C_{lg}$  the liquid-gate capacitance<sup>19</sup>. To understand the origin of the two different regimes, one has to see that the NW-FET resistance  $R = 1/G$  is composed of two resistances in series. The intrinsic NW resistance  $R_{NW}$  and the contact resistance  $R_c$ . Due to the confinement of the liquid channel to the nanowire,  $R_c$  is only weakly affected by the liquid gate (small  $C_{lg}$ ). Hence, if  $R_c$  dominates  $R$ ,  $C_{bg}/C_{lg}$  is large, which corresponds to the lower regime with  $V_{ref} < 0.4 \text{ V}$ . In contrast, if  $R_c$  can be neglected,  $R$  is determined by  $R_{NW}$ , which on its own is more strongly capacitively coupled to the liquid than to the back-gate. We refer to the two regimes as contact and NW dominated.

Figure 2 shows the frequency dependence of the noise power  $S_V(f)$  of the NW for different resistance values, measured in air (a) and in a buffer solution with pH 7 (b). The corresponding thermal background noise, recorded at zero bias, has been subtracted from the data. An example is shown by ( $\Delta$ ).  $S_V(f)$  has a clear  $1/f$  dependence (dashed lines), and its amplitude is proportional to

$V_{sd}^2$  (inset), as expected for  $1/f$  noise<sup>22</sup>. Such a behavior can phenomenologically be described by Hooge's law<sup>21,22</sup>

$$S_V(f) = V_{sd}^2 \frac{\alpha}{Nf}. \quad (1)$$

The material dependent parameter  $\alpha$  accounts for scattering effects and the constant  $N$  denotes the number of fluctuators in the system.

In Fig. 3, the normalized noise amplitude  $S_V/V_{sd}^2$  at 10 Hz is depicted as a function of  $R$ . The noise in the system increases dramatically (indicated by dashed lines) above a certain threshold resistance value. The position of this threshold (arrows) and the steepness of the rise depends on whether the NW is gated by the liquid or the back-gate. In air ( $\blacktriangledown$ ), where  $V_{bg}$  is the only applied gate voltage, the noise starts to increase at roughly 30 M $\Omega$ . A similar behavior is observed in liquid in the contact-dominated regime, i.e. for  $V_{ref} = -0.3$  V ( $\blacksquare$ ). In contrast, within the NW-dominated regime ( $\bullet$ ), the noise increases steeper, starting already at about 10 M $\Omega$ . For  $R$  smaller than the respective thresholds, the noise level is approximately constant. The apparent superimposed structure observed in this range is wire specific. Different NW-FETs, while confirming the general dependence, typically display a different fine structure. The thresholds of 10 – 30 M $\Omega$  correspond to the transition from the linear to the subthreshold regime of the FETs.

The physical signal in FET sensors is the shift  $\Delta V_{th}$  of the threshold voltage  $V_{th}$  caused by a chemical change on the sensing surface. It is obtained from the measured conductance change  $\Delta G$  and the transconductance  $g = G' = dG(V_g)/dV_g$ , characteristic for a given FET, as  $\Delta V_{th} = \Delta G/g$ . This equation can be used to determine the true figure of merit which is the equivalent noise power of the threshold voltage  $\delta V_{th}$  given by

$$\delta V_{th} = \frac{\sqrt{S_V/V_{sd}^2(f)}}{g/G} = \frac{\sqrt{S_V/V_{sd}^2(f)}}{(\ln G)'}. \quad (2)$$

Here, we have made use of the relation  $\delta G/G = \sqrt{S_V/V_{sd}}$ .

In Fig. 4a we show  $\delta V_{th}$  when the controlling gate is  $V_{bg}$  for data measured in air ( $\blacktriangledown$ ) together with the data acquired in buffer solution at  $V_{ref} = -0.3$  V ( $\blacksquare$ ). Both curves show a very similar behavior. Since we know that the liquid data obtained at  $V_{ref} = -0.3$  V is contact dominated, we conclude that the measurement in air is also contact dominated.

In Fig. 4b we summarize  $\delta V_{th}$  for measurements done in an electrolyte. To obtain  $\delta V_{th}$ , we consistently use  $V_{lg}$  as the controlling gate for all three data sets in this figure. Interestingly, in the NW-dominated regime ( $\bullet$ )  $\delta V_{th}$  is much smaller than in the contact-dominated regime ( $\blacksquare$ ). The difference can amount to almost two orders of magnitude. Although the voltage noise values  $S_V$  are not much different in the two regimes (Fig. 3), the sensitivities in the true measurement quantity greatly differ. This shows that the transconductance values, and therefore the gate-coupling to the liquid, are crucial factors

determining the ultimate sensitivity. We also stress that  $\delta V_{th}$  can be low over an extended range of NW resistance values  $R$ , from  $\sim 1$  to 100 M $\Omega$ . This range covers the transition from the linear to the subthreshold regime. The lowest value of  $2 - 3 \cdot 10^{-5}$  V/ $\sqrt{\text{Hz}}$  corresponds to an accuracy of 0.5 ‰ of a typical Nernstian pH shift in one Hz bandwidth (right axis) throughout the full resistance range ( $\bullet$ ).

The data set obtained at a fixed  $V_{bg}$  and varying  $V_{ref}$  ( $\blacktriangle$ ) demonstrate the cross-over between the two different regimes. In this case a very pronounced transition from a regime with low sensitivity (low  $R$ ) to a regime with high sensitivity (larger  $R$ ) is apparent. For this case, it has recently been pointed out<sup>16</sup> that the signal-to-noise ratio (SNR) (corresponding to  $1/\delta V_{th}$ ) increases with resistance  $R$  and is the highest in the subthreshold regime. We confirm this as well but we emphasize that the dual-gate approach used here provides a more general and detailed insight. For  $V_{ref} = -0.3$  V, the contact leads also contribute to the total noise and strongly decrease the SNR. In contrast, for  $V_{ref} = +0.5$  V, the resistance of the NW-FET is not contact-dominated. In that case the SNR is constantly large over the whole resistance range.

As a last step, we estimate the minimum detectable number of charges  $Q_0$  at the NW sensing surface. To do so, we first relate the charge noise  $\delta Q_0$  to the respective quantity  $\delta Q$  for charges in the NW and then to the conductance noise  $\delta G = G\sqrt{S_V}/V_{sd}$  using the relations  $\delta Q/\delta Q_0 = C_{NW}/C_{DL}$  and  $\delta G = \delta Q\mu/L^2$ , where  $C_{NW}$ ,  $C_{DL}$ ,  $\mu$ , and  $L$  denote the density-of-state capacitance (quantum capacitance) of the NW, the double-layer capacitance, the mobility and the length of NW, respectively. In the subthreshold regime we have in addition  $C_{NW} = Q/(k_B T/e)$ , where  $T$  is the absolute temperature and  $k_B$  Boltzmann's constant<sup>16</sup>. This altogether yields

$$\delta Q_0 = \frac{k_B T}{e} C_{dl} \sqrt{\frac{S_V}{V_{sd}^2}}, \quad (3)$$

Using measured values for  $V_{ref} = +0.5$  V at 10 Hz and  $C_{dl} \approx 7 \cdot 10^{-12}$  F, we obtain  $\delta Q_0/e \approx 10^1 \dots 10^2 \sqrt{\text{Hz}}^{-1}$ .

In conclusion, we have studied the low-frequency noise in a dual-gated SiNW-FET sensor and the signal-to-noise ratio over a large resistance range. The deduced threshold voltage noise  $\delta V_{th}$  is an important quantity in a FET sensor and strongly depends on the working point. We stress that  $\delta V_{th}$  can be low over an extended range from the linear to the subthreshold regime, even though the voltage noise  $S_V$  grows non-linearly with resistance and is the highest in the subthreshold range. We also confirmed recent studies that found the SNR increasing with resistance in a certain case.

## Acknowledgments

The authors acknowledge the LMN at the PSI Villigen for the oxidation of the SOI wafers. We are grateful for

the support provided by the nano-tera.ch, Sensirion AG, and the Swiss Nanoscience Institute (SNI).

- 
- \* These authors contributed equally to this work  
<sup>†</sup> Electronic address: Christian.Schoenenberger@unibas.ch
- <sup>1</sup> P. Bergveld, Development of an ion-sensitive solid-state device for neurophysiological measurements. *IEEE Trans. Biomed. Eng.* **17**, 70 (1970).
  - <sup>2</sup> P. Bergveld, Thirty years of ISFETOLOGY - What happened in the past 30 years and what may happen in the next thirty years. *Sens. Actuators B* **88**, 1 (2003).
  - <sup>3</sup> S. Tans, A. Verschueren, C. Dekker, Room-temperature transistor based on a single carbon nanotube. *Nature* **393**, 49 (1998).
  - <sup>4</sup> J. Kong, N. Franklin, C. Zhou, M. Chapline, S. Peng, K. Cho, H. Dai, Nanotube molecular wires as chemical sensors. *Science* **287**, 622 (2000).
  - <sup>5</sup> P. Collins, K. Bradley, M. Ishigami, A. Zettl, Extreme oxygen sensitivity of electronic properties of carbon nanotubes. *Science* **287**, 1801 (2000).
  - <sup>6</sup> M. Krüger, M. R. Buitelaar, T. Nussbaumer, C. Schönenberger, Electrochemical Carbon Nanotube Field-Effect Transistor. *Appl. Phys. Lett.* **78**, 1291 (2001).
  - <sup>7</sup> P. Ang, W. Chen, A. Wee, and K. Ping, Solution-Gated Epitaxial Graphene as pH Sensor. *J. Am. Chem. Soc.* **130**, 14392 (2008).
  - <sup>8</sup> Y. Ohno, K. Maehashi, Y. Yamashiro, and K. Matsumoto, Electrolyte-Gated Graphene Field-Effect Transistors for Detecting pH and Protein Adsorption. *Nano Lett.* **9**, 3318 (2009).
  - <sup>9</sup> Z. Cheng, Q. Li, Z. Li, Q. Zhou, and Y. Fang, Suspended Graphene Sensors with Improved Signal and Reduced Noise. *Nano Lett.* **10**, 1864 (2010).
  - <sup>10</sup> X. Duan, Y. Huang, Y. Cui, J. Wang, C. Lieber, Indium phosphide nanowires as building blocks for nanoscale electronic and optoelectronic devices. *Nature* **409**, 66 (2001).
  - <sup>11</sup> Y. Cui, C. Lieber, Functional nanoscale electronic devices assembled using silicon nanowire building blocks. *Science* **291**, 851 (2001).
  - <sup>12</sup> E. Stern, J. F. Klemic, D. A. Routenberg, P. N. Wyrembak, D. B. Turner-Evans, A. D. Hamilton, D. A. LaVan, T. M. Fahmy, and M. A. Reed, Label-free immunodetection with CMOS-compatible semiconductor nanowires. *Nature* **445**, 519 (2007).
  - <sup>13</sup> N. Elfström, R. Juhasz, I. Sychugov, T. Engveldt, A. Eriksson, J. Linnros, Surface Charge Sensitivity of Silicon Nanowires: Size Dependence. *Nano Lett.* **7**, 2608 (2007).
  - <sup>14</sup> N. K. Rajan, D. A. Routenberg, J. Chen, and M. Reed, 1/f Noise of Silicon Nanowire BioFETs. *IEEE Electr. Device L.* **31**, 615 (2010).
  - <sup>15</sup> I. Heller, J. Männik, S. G. Lemay, and C. Dekker, Optimizing the Signal-to-Noise Ratio for Biosensing with Carbon Nanotube Transistors. *Nano Lett.* **9**, 2268 (2009).
  - <sup>16</sup> X. A. Gao, G. Zheng, C. Lieber, Subthreshold Regime has the Optimal Sensitivity for Nanowire FET Biosensors. *Nano Lett.* **10**, 547 (2010).
  - <sup>17</sup> O. Elibol, B. Reddy Jr., R. Bashir, Nanoscale thickness double-gated field effect silicon sensors for sensitive pH detection in fluid. *Appl. Phys. Lett.* **92**, 193904 (2008).
  - <sup>18</sup> O. Knopfmacher, D. Keller, M. Calame, C. Schönenberger, Dual Gated Silicon Nanowire Field Effect Transistors. *Proceedia Chem.* **1**, 678 (2009).
  - <sup>19</sup> O. Knopfmacher, A. Tarasov, W. Fu, M. Wipf, B. Niesen, M. Calame, C. Schönenberger, Nernst Limit in Dual-Gated Si-Nanowire FET Sensors. *Nano Lett.* **10**, 2268 (2010).
  - <sup>20</sup> Microsens SA, [http://www.microsens.ch/products/pdf/MSFET\\_datasheet%20.pdf](http://www.microsens.ch/products/pdf/MSFET_datasheet%20.pdf) (retrieved 17 September 2010).
  - <sup>21</sup> F. N. Hooge, 1/f noise is no surface effect. *Phys. Lett. A* **29**, 139 (1969).
  - <sup>22</sup> F. N. Hooge, T. G. M. Kleinpenning, L. K. J. Vandamme, Experimental studies on 1/f noise. *Rep. Prog. Phys.* **44**, 479 (1981).

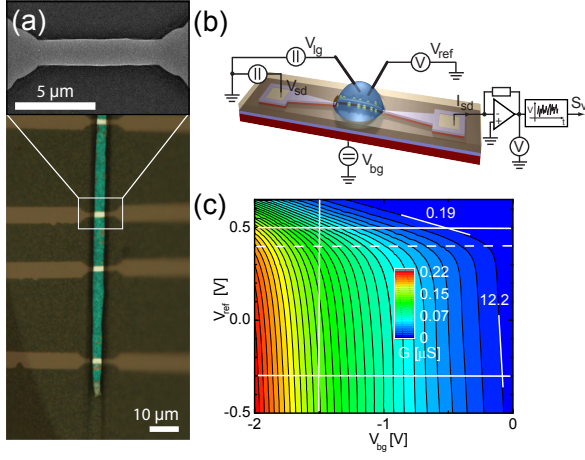


FIG. 1: (a) Optical image of a sample with four nanowires (NWs) (horizontal) and an enlarged SEM image of one of the NWs. The (vertical) liquid channel is the only part of the sample which is not covered with photoresist. (b) A schematic representation of the setup used for the measurements in liquid. There are two gates, a back-gate and a liquid-gate with applied gate voltages  $V_{bg}$  and  $V_{lg}$ . The liquid potential is measured by a calomel reference electrode and denoted as  $V_{ref}$ . The NW-FETs are characterized by their small-signal conductance map  $G(V_{bg}, V_{ref})$ , shown in (c), and by the noise obtained from the temporal dependence of the source-drain current  $I_{sd}$  using fast Fourier transform. In (c) the horizontal dashed line marks the border between two regimes, the NW (upper) and contact (lower) dominated regime. Noise measurements were conducted along the three solid white lines. Short solid lines and numbers represent the slopes of the equi-conductance lines.

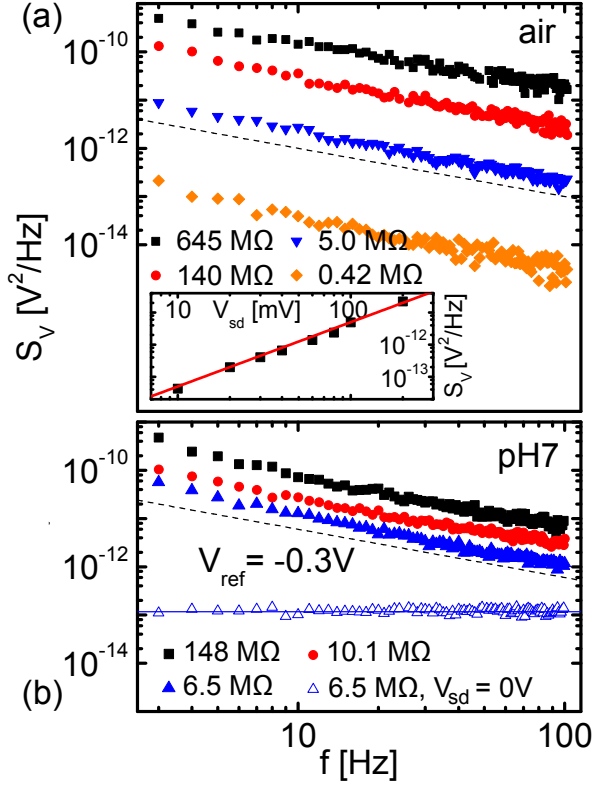


FIG. 2: The noise power spectral density of the voltage fluctuations  $S_V$  obtained for a source-drain bias voltage of  $V_{sd} = 90$  mV for different resistances of a NW measured (a) in air and (b) in a buffer solution (Titrisol pH 7, Merck). The dashed lines indicate a  $1/f$  slope. The open symbols in (b) represent the thermal noise of the NW at  $V_{sd} = 0$  V ( $\triangle$ ). The calculated thermal noise of a 6.5 M $\Omega$  resistor at 300 K is shown for comparison (horizontal line). Inset:  $S_V$  as a function of  $V_{sd}$  at 7 Hz, measured in air (logarithmic scale). The solid red line indicates a power law with exponent two.

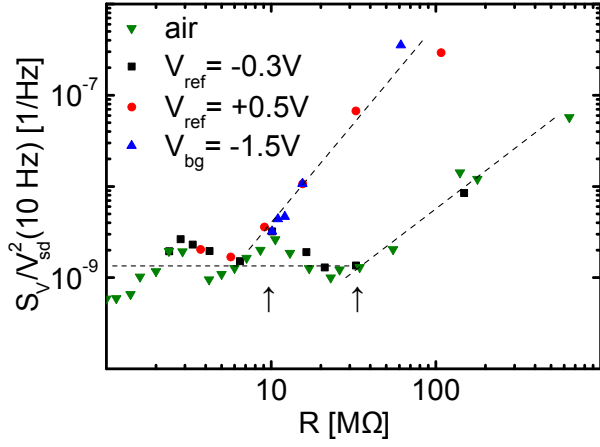


FIG. 3:  $S_V$  divided by the squared source-drain voltage  $V_{sd}^2$  as a function of  $R$  at 10 Hz, measured in air and in buffer solution (logarithmic scale). Dashed lines are guides to the eye. Arrows indicate the transition between different regimes.

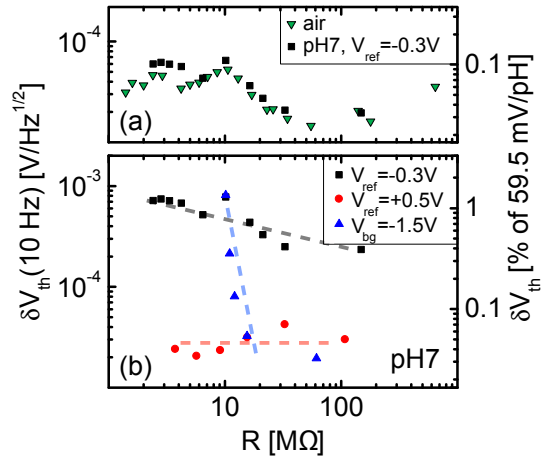


FIG. 4: Threshold voltage fluctuations  $\delta V_{th} = S_V / (\ln G(V_{bg}))'$  (a) and  $S_V / (\ln G(V_{ref}))'$  (b), calculated from the data in Fig. 3 as a function of  $R$ . Dashed lines are guides to the eye. The right axis shows  $\delta V_{th}$  relative to the Nernst limit of the pH sensitivity (59.5 mV/pH at 300 K).